Theoretical calculation of oxygen equilibrium isotope fractionation factors involving various NO_y molecules, $\cdot OH$, and H_2O and its implications for isotope variations in atmospheric nitrate

Wendell W. Walters [a,*], Greg Michalski [a,b]

[a] *Department of Earth, Atmospheric, and Planetary Sciences, Purdue University, 550 Stadium Mall Drive, West Lafayette, IN 47907, United States*
[b] *Department of Chemistry, Purdue University, 560 Oval Drive, West Lafayette, IN 47907, United States*

Abstract

The oxygen stable isotope composition ($\delta^{18}O$) of nitrogen oxides [NO_x = nitric oxide (NO) + nitrogen dioxide (NO_2)] and their oxidation products (NO_y = NO_x + nitric acid (HNO_3) + particulate nitrate (p-NO_3^-) + nitrate radical (NO_3) + dinitrogen pentoxide (N_2O_5) + nitrous acid (HONO) + ...) have been shown to be a useful tool for inferring the proportion of NO_x that is oxidized by ozone (O_3). However, isotopic fractionation processes may have an influence on $\delta^{18}O$ of various NO_y molecules and other atmospheric O-bearing molecules pertinent to NO_x oxidation chemistry. Here we have evaluated the impacts of O isotopic exchange involving NO_y molecules, the hydroxyl radical ($\cdot OH$), and water (H_2O) using reduced partition function ratios ($^x\beta$) calculated by hybrid density functional theory. Assuming atmospheric isotopic equilibrium is achieved between NO and NO_2 during the daytime, and NO_2, NO_3, and N_2O_5 during the nighttime, $\delta^{18}O$–$\delta^{15}N$ compositions were predicted for the major atmospheric nitrate formation pathways using our calculated exchange fractionation factors and isotopic mass-balance. Our equilibrium model predicts that various atmospheric nitrate formation pathways, including $NO_2 + \cdot OH \rightarrow HNO_3$, $N_2O_5 + H_2O + surface \rightarrow 2HNO_3$, and $NO_3 + R \rightarrow HNO_3 + R\cdot$ will yield distinctive $\delta^{18}O$–$\delta^{15}N$ compositions. Our calculated $\delta^{18}O$–$\delta^{15}N$ compositions match well with previous atmospheric nitrate measurements, and will potentially help better understand the role oxidation chemistry plays on the N and O isotopic composition of atmospheric nitrate.
© 2016 Elsevier Ltd. All rights reserved.

Keywords: NO_x; Nitrate; Isotopes; Isotope Exchange; Equilibrium; Fractionation

1. INTRODUCTION

Stable isotopes are useful for understanding complex chemical systems such as the cycling and oxidation of NO_x [NO_x = nitric oxide (NO) + nitrogen dioxide (NO_2)]. For example, the oxygen (O) stable isotope composition of atmospheric nitrate, which includes nitric acid (HNO_3), nitrate (NO_3^-), and particulate nitrate (p-NO_3^-), indicates the proportion of NO_x that reacts with ozone (O_3) during its oxidation (Michalski et al., 2003; Thiemens, 2006; Savarino et al., 2007; McCabe et al., 2007; Morin et al., 2008; Alexander et al., 2009). The O isotope composition

of a sample is typically reported in delta notation (δ), which is expressed as the ratio of the heavy (^{17}O and ^{18}O) to the light (^{16}O) isotope in a sample relative to the same ratio of an international standard (Vienna Standard Mean Ocean Water (VSMOW):

$$\delta^x O(\text{‰}) = \left[\left(\frac{[^xO/^{16}O]_{sample}}{(^xO/^{16}O)_{VSMOW}} \right) - 1 \right] \times 1000 \qquad (1)$$

where x represents the abundance of either ^{17}O or ^{18}O. Several studies have shown that atmospheric O_3 has elevated $\delta^{17}O$ and $\delta^{18}O$ values relative to VSMOW and a strong mass-independent component (Thiemens and Heidenreich, 1983; Krankowsky et al., 1995; Johnston and Thiemens, 1997; Mauersberger et al., 2001; Vicars et al., 2012; Vicars and Savarino, 2014), which is quantified by $\Delta^{17}O$ notation:

$$\Delta^{17}O(\text{‰}) = 1000\ln\left[1 + \frac{\delta^{17}O}{1000}\right] - 0.52 \times 1000\ln\left[1 + \frac{\delta^{18}O}{1000}\right] \qquad (2)$$

These elevated $\delta^{18}O$ and $\Delta^{17}O$ signatures are transferred to atmospheric nitrate proportionally when O_3 oxidizes NO_x (Thiemens, 2006; Savarino et al., 2008; Michalski and Bhattacharya, 2009; Berhanu et al., 2012). Thus, O isotopic analysis, particularly $\Delta^{17}O$, of atmospheric nitrate has been suggested as a useful proxy for assessing changes in NO_x oxidation and for evaluating long-term changes in the atmosphere's oxidation capacity (e.g. Michalski et al., 2003; Alexander et al., 2009; Alexander and Mickley, 2015).

There may be additional useful information in $\delta^{18}O$ variations, because mass-dependent fractionation processes (MDFP) such as equilibrium or kinetic isotope effects will have a minimal impact on $\Delta^{17}O$ but may induce significant $\delta^{18}O$ variations. These fractionation processes may also influence the nitrogen (N) isotopic composition ($\delta^{15}N(\text{‰})$ $= [(^{15}N/^{14}N)_{sample}/(^{15}N/^{14}N)_{air} - 1] \times 1000$, where air N_2 is the N isotopic reference) as NO_x is oxidized to atmospheric nitrate (e.g. Freyer et al., 1993; Vicars et al., 2013; Walters et al., 2016). Thus, $\delta^{18}O$ and $\delta^{15}N$ of atmospheric nitrate may be related, reflecting to some degree the fractionation processes responsible for the formation of atmospheric nitrate. However, few studies have quantitatively evaluated the impacts of NO_x oxidation fractionation processes on $\delta^{18}O$ and their implications for possible $\delta^{18}O$–$\delta^{15}N$ relationships of the atmospheric nitrate end product.

One such fractionation process that may play an important role on the $\delta^{18}O$ and $\delta^{15}N$ of atmospheric nitrate is isotopic equilibrium exchange or partial exchange. For example, it has been previously suggested that isotopic equilibrium between NO and NO_2 has a significant impact on the $\delta^{15}N$ of HNO_3 produced during the daytime (Freyer et al., 1993; Riha, 2013; Vicars et al., 2013; Savarino et al., 2013; Walters et al., 2016). The same exchange processes may also generate useful $\delta^{18}O$ signatures in HNO_3. Additionally, it has been suggested that NO_2, the nitrate radical (NO_3), and dinitrogen pentoxide (N_2O_5) may reach isotopic equilibrium during the nighttime (Amell and Daniels, 1952; Freyer, 1991; Walters et al., 2016). Isotopic equilibrium involving NO_2, NO_3, and N_2O_5 will affect partitioning of ^{18}O and ^{15}N between these molecules, which has

implications for variations in $\delta^{18}O$ and $\delta^{15}N$ of HNO_3 produced at night. Thus, isotopic equilibrium exchange in addition to mass-balance considerations may have important implications for diurnal and seasonal variations in $\delta^{18}O$–$\delta^{15}N$ compositions of atmospheric nitrate. In this case, knowing the isotopic equilibrium fractionation factors involving a variety of oxidized N molecules (denoted as $NO_y = NO_x + HNO_3 + p\text{-}NO_3^- + NO_3 + N_2O_5 + $ nitrous acid (HONO) $+ \ldots$) would be useful.

Prior studies have calculated O isotopic equilibrium exchange fractionation factors involving some NO_y molecules using measured vibrational spectroscopic data (Richet et al., 1977) or empirically determined interatomic force constants (Stern et al., 1968; Monse et al., 1969). However, O isotopic equilibrium fractionation factors have not been determined for many atmospherically relevant NO_y molecules such as N_2O_5, NO_3, and halogen nitrates ($XONO_2$). This is primarily due to the absence of spectroscopic data for the isotopologues of these molecules. Previously, we have used computational quantum chemistry methods to calculate N isotopic equilibrium fractionation factors involving some NO_y molecules (Walters and Michalski, 2015). Here we will extend that study and calculate O isotopic equilibrium exchange fractionation factors for singly substituted O isotopologues of numerous NO_y molecules. We will also calculate the fractionation factor associated with equilibrium isotopic exchange between the hydroxyl radical (·OH) and water (H_2O) due to the importance this reaction has on the $\delta^{18}O$ of atmospheric ·OH (Dubey et al., 1997; Lyons, 2001; Michalski et al., 2012). Knowing $\delta^{18}O$ of ·OH is important because it will be transferred proportionally to the atmospheric nitrate end product from ·OH reaction with NO_2 (Michalski et al., 2012). Our calculated O isotopic equilibrium fractionation factors will allow for the evaluation of the impact various exchange reactions have on $\delta^{18}O$ values of these molecules and how it may be propagated into the atmospheric nitrate end product. Combining our O and N isotopic equilibrium fractionation factors will allow for the prediction of $\delta^{18}O$–$\delta^{15}N$ arrays resulting from various atmospheric nitrate formation pathways.

2. METHODS AND THEORY

2.1. Calculation of equilibrium isotope exchange fractionation factors

The theoretical calculation of isotopic fractionation associated with isotope exchange equilibrium reactions has long been carried out in the harmonic approximation using partition functions (Urey, 1947; Bigeleisen and Mayer, 1947). In the Born–Oppenheimer, harmonic oscillator, and rigid-rotor approximations, the reduced partition function ratio (RPFR, commonly denoted as $^x\beta$) for an oxygen isotopic pair is written as:

$$RPFR = {}^x\beta_{har} = \prod_i^N \frac{u_2}{u_1} \times \exp\left(\sum_i^N \frac{u_{1i} - u_{2i}}{2}\right)$$
$$\times \prod_i^N \frac{1 - \exp(-u_{1i})}{1 - \exp(-u_{2i})} \qquad (3)$$

where x and subscript 2 refer to one of the heavy isotopes (^{17}O or ^{18}O) and subscript 1 refers to ^{16}O. The $u_i = hc\omega_i/kT$ where h is Planck's constant, c is the speed of light, ω_i is the harmonic frequency (cm^{-1}) for each vibrational mode (i), k is Boltzmann constant, T is temperature in Kelvin, and N refers to the number of normal mode vibrational frequencies. In Eq. (3), the Teller–Redlich rule was employed (Redlich, 1935), which converts translational and rotational motion into vibrational frequencies. Symmetry numbers are not considered, because symmetry in itself does not lead to isotopic enrichment during equilibrium (Bigeleisen and Mayer, 1947) but must be considered from a statistical perspective (Coulson, 1978; Pollak and Pechukas, 1978; Michalski and Bhattacharya, 2009).

The $^x\beta$ values calculated using Eq. (3) are accurate in the harmonic oscillator and rigid-rotor approximations. However, corrections for anharmonicity, vibration–rotation coupling, centrifugal distortion, hindered internal rotation, and quantum mechanical correction to rotation have been shown to be important for calculating accurate $^x\beta$ values for some molecules (Pennington and Kobe, 1954; Richet et al., 1977; Liu et al., 2010). Generally, for atoms other than H most of the corrections can be ignored as $^x\beta$ is impacted by less than 0.01‰. The main exception is anharmonic correction to the zero point energy (ZPE), which can play a significant role in the calculation of accurate $^x\beta$ values (Liu et al., 2010). If accurate ZPEs are known or can be accounted for, $^x\beta$ values can more accurately be calculated by the following (Liu et al., 2010):

$$^x\beta_{anhar} = \frac{\exp[-ZPE_{anhar,2}/kT]}{\exp[-ZPE_{anhar,1}/kT]} \prod_i^N \left[\frac{u_2}{u_1}\right] \times \left[\frac{1 - \exp(-u_{1i})}{1 - \exp(-u_{2i})}\right]$$
(4)

where ZPE_{anhar} is the anharmonic corrected ground ZPE.

A general representation for an equilibrium isotope exchange reaction involving two different chemical compounds, A and B, is:

$$A_1 + B_2 \leftrightarrow A_2 + B_1$$
(5)

where subscripts 1 and 2 again refer to the light and heavy isotopologue, respectively. The equilibrium constant, $^xK_{A/B}$, which is also called the equilibrium isotope fractionation factor ($^x\alpha_{A/B}$), can be obtained from the $^x\beta$ values of A and B:

$$^xK_{A/B} = {}^x\alpha_{A/B} = \frac{^x\beta_A}{^x\beta_B}$$
(6)

For example, using this notation, the equilibrium isotope exchange reaction between NO and NO$_2$ involving the singly substituted ^{18}O and ^{16}O isotopologue pair is written as:

$$N^{18}O + N^{16}O^{16}O \leftrightarrow N^{16}O + N^{16}O^{18}O$$
(7)
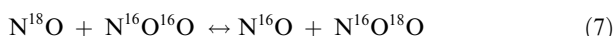
The equilibrium constant for this isotope exchange reaction is written as:

$$^{18}K_{NO_2/NO} = {}^{18}\alpha_{NO_2/NO} = \frac{^{18}\beta_{NO_2}}{^{18}\beta_{NO}}$$
(8)

2.2. Computational chemistry methods

Using *ab initio* methods to obtain β and $\alpha_{A/B}$ values for use in geochemical systems is a relatively recent advance (e.g., Driesner et al., 2000; Yamaji et al., 2001; Schauble et al., 2004, 2006; Anbar et al., 2005; Liu and Tossell, 2005; Otake et al., 2008; Liu et al., 2010). In this study, the Becke-3 parameter-Lee–Yang–Parr (B3LYP) hybrid density function theory (DFT) method (Lee et al., 1988; Becke, 1993) and Dunning correlation-consistent polarized valence triple ζ (cc-pVTZ) basis set (Dunning, 1989) were used to calculate geometries (bond angles and bond lengths) and harmonic frequencies for the following molecules: NO, NO$_2$, HONO, HNO$_3$, N$_2$O$_5$, nitrate (NO$_3^-$), chlorine nitrate (ClONO$_2$), nitrite (NO$_2^-$), dinitrogen tetroxide (N$_2$O$_4$), nitryl bromide (BrNO$_2$), nitryl chloride (ClNO$_2$), bromine nitrate (BrONO$_2$), ·OH, and H$_2$O. We also calculated the geometry and vibrational frequencies of NO$_3$ using the EDF2 DFT method (Lin et al., 2004) with the cc-pVTZ basis set (EDF2/cc-pVTZ) and the QCISD method with the cc-pVDZ basis set (QCISD/cc-pVDZ). These additional methods were used to compare the calculated vibrational frequencies of NO$_3$ due to the difficulties this molecule presents for computational studies related to it being a polyatomic doublet radical with multireference character (e.g. Morris et al., 1990; Dutta et al., 2013). Calculations involving the B3LYP/cc-pVTZ and QCISD/cc-pVDZ methods were performed using the Gaussian09 program package revision D.01 (Frisch et al., 2009) on the Purdue Radon cluster (ITaP Research Computing, 2015). The EDF2/cc-pVTZ calculations were performed using the QCHEM 4.2 program package (Shao et al., 2015) on an IBM personal computer.

The masses of the most abundant isotopes of each element (^1H, ^{12}C, ^{14}N, ^{16}O, ^{35}Cl, ^{79}Br) were used to calculate harmonic frequencies, and isotope effects were subsequently determined via single-atom substitutions of either ^{17}O or ^{18}O for each ^{16}O position. Systematic model errors and anharmonic corrections to the ZPE were accounted for by applying a constant scale factor to the calculated harmonic ZPE, as recommended by Liu et al. (2010). We used a constant scale factor of 0.9787, recommended by Sinha et al. (2004) to correct calculated harmonic ZPE using B3LYP/cc-pVTZ to match experimental ZPEs. This scale factor was also used to correct the ZPE of NO$_3$ calculated using EDF2/cc-pVTZ. The ZPE of NO$_3$ calculated from QCISD/cc-pVDZ was scaled by 0.9776, based on a recommended value for QCISD/6-31G(d) (Scott and Radom, 1996).

3. RESULTS

3.1. Calculated $^x\beta$ values

Calculated geometries (Table S1), harmonic frequencies (Table S2), and ZPEs (Table S3) for the molecules of interest in this study are presented in the Supplementary data. The NO$_3$ vibrational frequencies calculated using B3LYP/cc-pVTZ, EDF2/cc-pVTZ, QCISD/cc-pVDZ, and EOM-CCSD/aug-cc-pVDZ (Walters and Michalski, 2015)

Table 1

Comparison of calculated NO_3 v_i (cm^{-1}) from different computational methods and experimental determined values. Values in parentheses represent the absolute difference between the calculated and experimental frequency for a particular vibrational mode.

	v_1 (asym bend)	v_2 (asym bend)	v_3 (umbrella)	v_4 (sym stretch)	v_5 (asym stretch)	v_6 (asym stretch)	Average error[*]
B3LYP/cc-pVTZ[a]	204.93 (160.7)	206.64 (159.0)	809.25 (46.2)	1107.09 (54.1)	1108.04 (8.0)	1129.61 (29.6)	76.3
EDF2/cc-pVTZ[a]	337.75 (27.9)	339.79 (25.8)	816.47 (53.4)	1142.11 (89.1)	1171.90 (71.9)	1174.35 (74.3)	57.1
QCISD/cc-pVDZ[a]	201.82 (163.8)	203.80 (161.8)	813.92 (50.8)	1144.00 (91.0)	1168.86 (68.9)	1169.08 (69.1)	100.9
EOM-CCSD/ aug-cc-pVDZ[b]	310.80 (54.8)	312.94 (52.7)	743.37 (19.7)	1103.92 (50.9)	1263.96 (164.0)	1264.34 (164.3)	84.4
Experiment	365.6[c]	365.6[c]	763.1[d]	1053.0[e]	1100.0[c]	1100.0[c]	

[a] Calculated from this work.
[b] Calculated previously from Walters and Michalski (2015).
[c] Beckers et al. (2009).
[d] Kim et al. (1992).
[e] Jacox and Thompson (2008).
[*] Calculated as the average absolute deviation from experimental vibrational frequencies (i): $\frac{1}{6}\sum_{i=1}^{6}|(v_1)_{calculated} - (v_i)_{experiment}|$.

were compared (Table 1) with experimental data (Kim et al., 1992; Jacox and Thompson, 2008; Beckers et al., 2009). Generally, it is found the most accurate NO_3 vibrational frequencies are from the EDF2/cc-pVTZ method (Table 1). Using calculated frequencies, $^x\beta$ values were calculated for each molecule over a temperature range from 150 to 450 K using Eq. (4). For the molecules that had non-equivalent O sites (i.e. HNO_3, N_2O_5, $ClONO_2$, HONO, and $BrONO_2$), two $^x\beta$ values were calculated. These are designated as "c" to refer to the substitution of ^xO in the central bridging O atom position (e.g. $HONO^c = H^xONO$) and "t" to refer to the substitution of ^xO in the terminal O atom position (e.g. $HONO^t = HON^xO$). For molecules with more than one terminal O atom, but with slight break in symmetry (e.g. HNO_3, $BrONO_2$, and $ClONO_2$), the geometric mean $^x\beta$ at all terminal sites is reported. These terminal sites are nearly equivalent as their O $^x\beta$ values were generally within 0.001.

Regression fit parameters calculated for $^{18}\beta$ as a function of temperature, and $^{18}\beta$ values at 298 K, are reported in Table 2. Calculated $^{17}\beta$ regression fit parameters and values at 298 K can be found in the Supporting data (Table S4). At 298 K, $^{18}\beta$ ranged from 1.0258 to 1.1110, increasing in the following order: $\cdot OH < H_2O < BrONO_2^c < ClONO_2^c < N_2O_5^c < HONO^c < NO_3 < HNO_3^c < NO_3^- < NO_2 < NO_2^- < N < N_2O_4 < BrNO_2 < ClNO_2 < HNO_3^t < HONO^t < BrONO_2^t < ClONO_2^t < N_2O_5^t$ (Table 2). The magnitude of $^{18}\beta$ appears to be related to the number of bonds and the electronegativity of the oxygen bond-partner and increased in the following order: 1 hydrogen < 2 hydrogen < 1 halogen + 1 nitrogen < 2 nitrogen < 1 hydrogen + 1 nitrogen < 1 nitrogen (Table 2). This ordering of atoms that O is directly bonded to may provide a rough a priori way to arrange $^{18}\beta$ values based solely on molecular structure.

Fig. 1 compares our calculated $^{18}\beta$ values for NO, NO_2, H_2O, and HNO_3^c with those previously reported (Monse et al., 1969; Richet et al., 1977; Liu et al., 2010) as well as calculated using experimental data (Michalski, 2003; Michalski et al., 2004). Overall, our calculated $^{18}\beta$ values agree with those previously reported (Fig. 1). For example, at 300 K, we calculated $^{18}\beta_{(NO)}$ to be 1.0995, which is close

to previously calculated values of 1.0973 (Richet et al., 1977) and 1.0963 (Monse et al., 1969). Additionally, our calculated $^{18}\beta_{(NO2)}$ at 300 K is 1.0909, which is close to the value of 1.0899 previously calculated by Monse et al. (1969) and the value of 1.0867 calculated from empirically determined interatomic force constants (Michalski, 2003) and experimental ZPEs (Michalski et al., 2004). For H_2O, we calculated $^{18}\beta_{(H2O)}$ at 300 K to be 1.0635, which is close to values previously calculated of 1.0632 (Liu et al., 2010) and 1.0630 (Richet et al., 1977). Finally, for HNO_3^c, we calculated $^{18}\beta(HNO_3^c)$ to be 1.0862 at 300 K, which is close to the value of 1.0860 reported by Monse et al. (1969). Fig. 2 compares the $^{18}\beta$ calculated for NO_3 using B3LYP/cc-pVTZ, EDF2/cc-pVTZ, and QCISD/cc-pVDZ methods and indicates general agreement. For example, at 300 K, $^{18}\beta$ for NO_3 is calculated to be 1.0775, 1.08135, and 1.0796 for B3LYP/cc-pVTZ, EDF2/cc-pVTZ, and QCISD/cc-pVDZ, respectively. However, since EDF2/cc-pVTZ calculated the most accurate NO_3 vibrational frequencies of the considered computational methods (Table 1), we used the EDF2/cc-pVTZ calculated $^{18}\beta$ values for $^{18}\alpha_{A/B}$ calculations involving NO_3.

3.2. Calculated $^{18}\alpha_{A/B}$ values

Using our calculated $^{18}\beta$ values, $^{18}\alpha_{A/B}$ were calculated for the following exchange reactions (A/B): NO/NO_2, NO_2/NO_3, $N_2O_5^{geo}/NO_2$, N_2O_4/NO_2, $BrNO_2/NO_2$, $ClNO_2/NO_2$, $BrONO_2^t/NO_2$, $ClONO_2^t/NO_2$, NO_3^-/H_2O, and $H_2O/\cdot OH$ over the temperature range of 150–450 K, where "geo" refers to the geometric mean $^{18}\beta$. These exchange reactions were chosen due to their common molecular structure (e.g. NO, NO_2, or OH subunits), and therefore, possibility that O isotopic exchange might occur at a rate comparable to the atmospheric lifetime of these compounds (~1 week). Few studies have experimentally determined $\alpha_{A/B}$ involving the considered molecules, limiting our ability to evaluate our calculated $\alpha_{A/B}$ values. One study that we are aware of involves the O isotopic exchange between NO_3^- and H_2O (Böhlke et al., 2003), in which $\alpha_{NO3-/H2O}$ was determined to be 1.0215 and 1.0131 at 295 K and

Table 2
Calculated $^{18}\beta$ regression coefficients as a function of temperature (150 K $\leqslant$ T $\leqslant$ 450 K) and $^{18}\beta$ (298 K) values for NO$_y$ molecules, ·OH, and H$_2$O.

$$1000(^{18}\beta - 1) = \frac{A}{T^4} \times 10^{10} + \frac{B}{T^3} \times 10^8 + \frac{C}{T^2} \times 10^6 + \frac{D}{T} \times 10^4$$

	A	B	C	D	$^{18}\beta$ (298 K)
·OH	1.1036	−1.9577	1.2889	0.51636	1.0258
H$_2$O	3.2070	−5.7294	3.9525	1.1030	1.0639
BrONO$_2^c$	2.1489	−6.1744	8.3297	−0.22623	1.0656
ClONO$_2^c$	2.6464	−7.0231	8.6922	−0.22784	1.0671
N$_2$O$_5^c$	2.6369	−6.9058	8.6047	−0.20778	1.0672
HONO^c	3.3651	−7.2949	7.0520	0.51606	1.0734
NO$_3^*$	6.7853	−13.499	11.279	−0.08248	1.0818
HNO$_3^c$	3.9484	−8.8137	9.0903	0.38699	1.0871
NO$_3^-$	6.3617	−13.388	12.124	−0.10652	1.0904
NO$_2$	7.8475	−15.028	11.690	0.20838	1.0918
NO$_2^-$	7.8614	−15.049	11.700	0.20718	1.0918
NO	8.1294	−14.507	10.124	0.93160	1.008
N$_2$O$_4$	7.7029	−14.916	12.695	0.21039	1.1034
BrNO$_2$	7.9945	−15.453	13.127	0.19084	1.1060
ClNO$_2$	8.0617	−15.674	13.396	0.19632	1.1084
HNO$_3^t$	7.9932	−15.922	13.776	0.10526	1.1086
HONO^t	8.5480	−16.103	12.686	0.50745	1.1099
BrONO$_2^t$	8.0302	−15.747	13.703	0.14583	1.1099
ClONO$_2^t$	8.0808	−15.824	13.748	0.16979	1.1110
N$_2$O$_5^t$	8.1801	−15.985	13.792	0.17181	1.1110

"c" and "t" correspond to the substitution of ^{18}O at the bridging or terminal O atom position, respectively for a particular molecule (e.g. HONO^c = H^{18}ONO, HONO^t = HON^{18}O).
Typical misfit in the regression is <0.01‰.
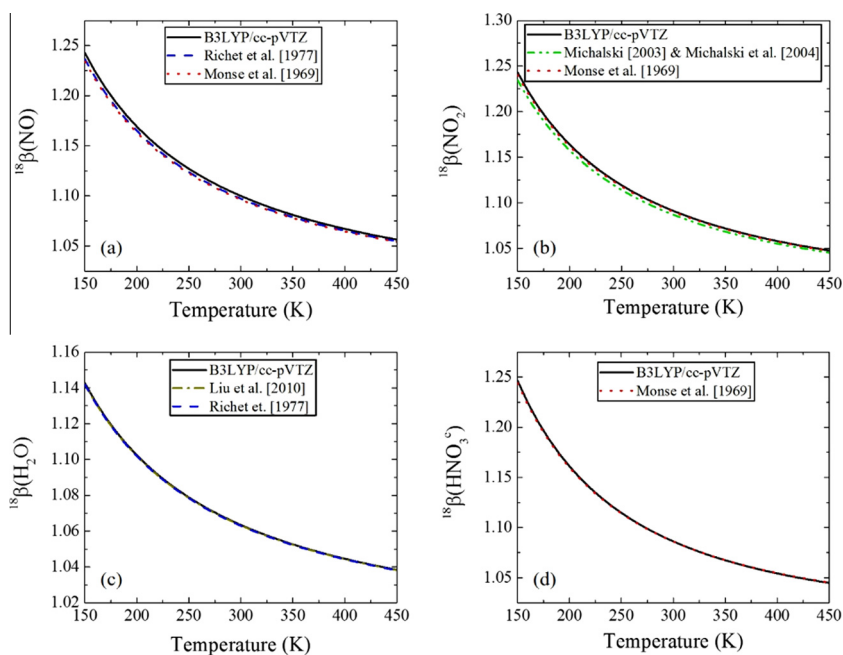[*] All $^{18}\beta$ values calculated using B3LYP/cc-pVTZ, except for NO$_3$, which was calculated using EDF2/cc-pVTZ.

Fig. 1. Comparison of calculated $^{18}\beta$ values using B3LYP/cc-pVTZ with those computed in previous studies for (a) NO (Monse et al., 1969; Richet et al., 1977), (b) NO$_2$ (Monse et al., 1969; Michalski, 2003; Michalski et al., 2004), (c) H$_2$O (Richet et al., 1977; Liu et al., 2010), and (d) HNO$_3^c$ (Monse et al., 1969).

373 K, respectively. These experimentally determined values agree reasonably well with our calculated values of 1.0256 and 1.0126 at 295 K and 373 K, respectively.

Table 3 presents the calculated $^{18}\alpha_{A/B}$ regression fit coefficients for these exchange reactions sorted in order of increasing $^{18}\alpha_{A/B}$ at 298 K. Overall, the calculated $^{18}\alpha_{A/B}$
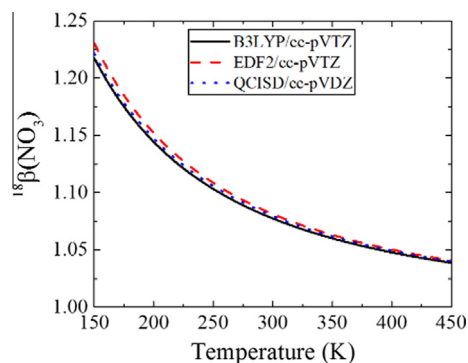
Fig. 2. Comparison of calculated $^{18}\beta$ for NO_3 using various computational methods that include B3LYP/cc-pVTZ, EDF2/cc-pVTZ, and QCISD/cc-pVDZ.

values ranged from 1.0082 to 1.0371 at 298 K (Table 3) and increased in the following order: $NO/NO_2 < NO_2/NO_3 < N_2O_5^{geo}/NO_2 < N_2O_4/NO_2 < BrNO_2/NO_2 < ClNO_2/NO_2 < BrONO_2^t/NO_2 < ClONO_2^t/NO_2 < NO_3^-/H_2O < H_2O/\cdot OH$ (Table 3). This trend indicates that at the most exchangeable sites (i.e. terminal O atoms), ^{18}O will generally partition into NO_y molecules other than NO and NO_2. This is true for all considered equilibrium exchange reactions except for NO_2/NO_3, in which ^{18}O is found to prefer NO_2. Additionally, our calculations indicate that the exchange between $H_2O/\cdot OH$ will result in atmospheric $\cdot OH$ depleted in ^{18}O relative to local H_2O vapor by approximately $-35‰$ at 298 K.

Fig. 3 displays the isotopic equilibrium exchange enrichment factors ($^{18}\varepsilon_{A/B} = 1000(^{18}\alpha_{A/B} - 1)$) for the following five isotopic equilibrium exchange reactions: NO/NO_2, NO_2/NO_3, $N_2O_5^{geo}/NO_2$, $ClNO_2/NO_2$, and $ClONO_2^t/NO_2$. Generally, as temperature increases, it is observed that $^{18}\varepsilon_{A/B}$ decreases towards zero as expected for equilibrium isotope effects in the high temperature limit. This was the observed trend for all of the considered isotopic exchange reactions except for NO/NO_2, in which $\alpha_{A/B}$ switches from less than 1 to greater than 1 at approximately 152.5 K. Fig. 3 also shows $\Delta^{17}O$ arising from the considered isotopic

equilibrium exchange reactions where $\Delta^{17}O$ was calculated according to the following:

$$\Delta^{17}O(‰) = 1000 \ln \left[1 + \left(^{17}\alpha_{A/B} - 1\right)\right]$$
$$- 0.52 \times 1000 \ln \left[1 + \left(^{18}\alpha_{A/B} - 1\right)\right] \quad (9)$$

For the considered exchange reactions, $\Delta^{17}O$ was found to minimally deviate from 0‰ (Fig. 3), ranging from 0.02 to 0.18‰ (Fig. 3) at 298 K.

4. DISCUSSION

Overall, our $^{18}\alpha_{A/B}$ calculations show that if isotopic equilibrium is achieved, it will influence the partitioning of ^{18}O between the considered molecules, without inducing a significant $\Delta^{17}O$ signature, as expected for a MDFP (Fig. 3). Therefore, while $\Delta^{17}O$ of NO_y molecules should approximately represent the O mass-balance of precursor molecules (i.e. O_3, H_2O, O_2), $\delta^{18}O$ may reflect both O mass-balance *and* possible influences from MDFP such as isotopic equilibrium exchange. Thus, $\delta^{18}O$ of NO_y molecules may provide additional information about NO_x oxidation pathways that is not observable in $\Delta^{17}O$ alone. Taking into account N and O isotopic mass-balance and assuming daytime isotopic equilibrium between NO and NO_2 (Freyer et al., 1993; Riha, 2013; Vicars et al., 2013; Savarino et al., 2013; Walters et al., 2016) and nighttime isotopic equilibrium between NO_2, NO_3, and N_2O_5 (Amell and Daniels, 1952; Freyer, 1991; Walters et al., 2016), $\delta^{18}O–\delta^{15}N$ compositions may be estimated for various HNO_3 formation pathways.

4.1. Predicted daytime HNO_3 $\delta^{18}O–\delta^{15}N$ compositions

During the daytime, NO_x exists in a photochemical steady state in which NO is oxidized to NO_2, which may photolyze back to NO leading to the production of O_3 (Leighton, 1961).

$$NO + O_3 \rightarrow NO_2 + O_2 \quad (R1)$$

$$NO_2 + h\nu \rightarrow NO + O(^3P) \quad (R2)$$

$$O(^3P) + O_2 + M \rightarrow O_3 + M \quad (R3)$$

Table 3
Calculated $^{18}\alpha_{A/B}$ regression coefficients as a function of temperature ($150\,K \leqslant T \leqslant 450\,K$) and $^{18}\alpha_{A/B}$ (298 K) values for O isotopic equilibrium exchange reactions.

$$1000(^{18}\alpha_{A/B} - 1) = \frac{A}{T^4} \times 10^{10} + \frac{B}{T^3} \times 10^8 + \frac{C}{T^2} \times 10^6 + \frac{D}{T} \times 10^4$$

	A	B	C	D	$^{18}\alpha_{A/B}$(298 K)
NO/NO_2	−0.04129	1.1605	−1.8829	0.74723	1.0082
NO_2/NO_3	1.03163	−1.38703	0.24875	0.3082	1.0092
$N_2O_5^{geo}/NO_2$	−0.54136	0.13073	1.2477	−0.1272	1.0096
N_2O_4/NO_2	−0.02333	−0.36888	1.0789	−0.00256	1.0106
$BrNO_2/NO_2$	0.29493	−0.96875	1.5039	−0.02007	1.0130
$ClNO_2/NO_2$	0.41012	−1.2744	1.7759	−0.01414	1.0152
$BrONO_2^t/NO_2$	0.43126	−1.4765	2.1167	−0.06681	1.0166
$ClONO_2^t/NO_2$	0.48353	−1.5568	2.1511	−0.04177	1.0176
NO_3^-/H_2O	3.6280	−8.6540	8.2763	−1.1983	1.0249
$H_2O/\cdot OH$	2.1137	−3.8026	2.5653	0.59410	1.0371

"t" corresponds to the substitution of ^{18}O at the terminal O atom position for a particular molecule (e.g. $BrONO_2^t = BrONO*O$) and "geo" refers to the geometric mean $^{18}\beta$ value for central and terminal mono-substituted ^{18}O of N_2O_5
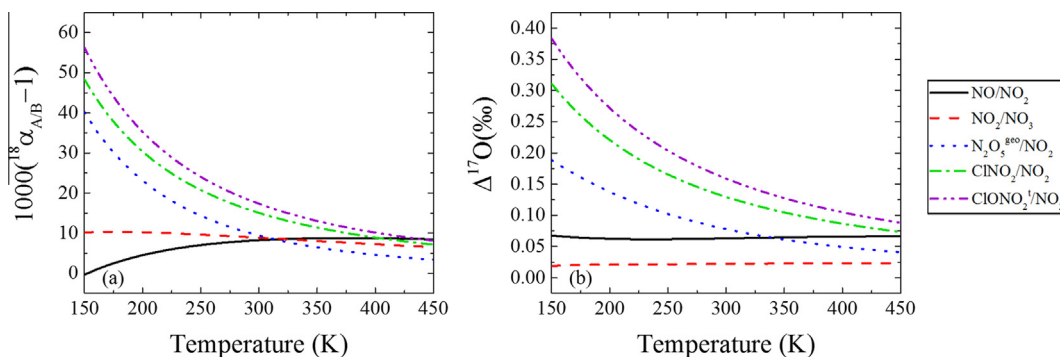Typical misfit in the regression is <0.01‰.

Fig. 3. (a) Calculated O isotopic exchange enrichment factors ($1000(^{18}\alpha_{(A/B)} - 1)$)) and (b) calculated O isotopic exchange induced mass-independence ($\Delta^{17}O(\text{‰}) = 1000\ln(^{17}\alpha_{(A/B)} - 1) - 0.52 * 1000\ln(^{18}\alpha_{(A/B)} - 1)$) for the following exchange reactions: NO/NO_2, NO_2/NO_3, $N_2O_5^{geo}/NO_2$, $ClNO_2/NO_2$, and $ClONO_2^{t}/NO_2$.

The photochemical cycling between NO–NO_2–O_3 is rapid, and prior experimental investigations of this cycling has suggested that O isotopic equilibrium is achieved between O_3 and NO_x (Michalski et al., 2014). Based on a photochemical NO_x–O_3 isotope equilibrium model, $\delta^{18}O$–NO_x has been estimated to have a value of $117 \pm 5\text{‰}$ relative to VSMOW (Michalski et al., 2014). While $\delta^{18}O$–NO_x is assumed to reflect its photochemical equilibration with O_3, $\delta^{15}N$–NO_x should be related to local NO_x source emissions. Recently, a mass-balance $\delta^{15}N$–NO_x model across the contiguous United States has been developed that suggests $\delta^{15}N$–NO_x should typically range from -15–0‰ (Walters et al., 2015). Exceptions include regions dominated by soil emissions (e.g. Great Plains during the summer) or coal-fired power plant emissions, in which $\delta^{15}N$–NO_x is estimated to range from -31–-21‰ and 5–9‰, respectively (Walters et al., 2015).

While the isotopic composition of NO_x is approximately known, the isotopic composition of its components, NO and NO_2, may be altered relative to NO_x due to isotopic exchange. The rate of isotopic exchange between NO and NO_2 is rapid ($k = 8.14 \times 10^{-14}$ cm^3 molecules^{-1}s^{-1} at 298 K; Sharma et al., 1970) and may lead to the partitioning of ^{18}O between NO and NO_2 similar to exchange previously observed for ^{15}N (Freyer et al., 1993; Walters et al., 2016). The resulting $\delta^{18}O$ and $\delta^{15}N$ of the NO and NO_2 will depend on the fraction of NO and NO_2 relative to the total NO_x (i.e. $[NO]/[NO_x]$ and $[NO_2]/[NO_x]$) and the temperature dependent equilibrium exchange fractionation factors (Freyer et al., 1993; Walters et al., 2016). The impact of this exchange on $\delta^{15}N$ of NO and NO_2 has been previously derived (Freyer et al., 1993; Walters et al., 2016), which we have adapted to also include $\delta^{18}O$, as the following:

$$\delta^x - NO_2(\text{‰}) = 1000\left[\frac{(^x\alpha_{NO_2/NO} - 1)(1 - f_{NO_2})}{(1 - f_{NO_2}) + (^x\alpha_{NO_2/NO} \cdot f_{NO_2})}\right]$$
$$+ \delta^x - NO_x(\text{‰}) \qquad (10)$$

$$\delta^x - NO(\text{‰}) = \frac{(\delta^x - NO_x(\text{‰})) - (f_{NO_2} \cdot \delta^x - NO_2(\text{‰}))}{(1 - f_{NO_2})}$$
$$(11)$$

where x represents either ^{18}O or ^{15}N and f_{NO2} is the fraction of NO_2 to the total NO_x. During the daytime, near equal concentrations of NO and NO_2 can occur (e.g. Vicars et al., 2013; Walters et al., 2016) due to the emission of NO (e.g. Gao, 2007) and NO_2 photolysis (Leighton, 1961). Therefore, during the daytime, $\delta^{18}O$ and $\delta^{15}N$ of NO and NO_2 will likely reflect a complex function of the $\delta^{18}O$ and $\delta^{15}N$ of NO_x and the NO_x equilibrium isotopic fractionation factors. If the isotopic composition of daytime NO_2 is altered relative to NO_x, it would have important consequences for $\delta^{18}O$ and $\delta^{15}N$ of atmospheric nitrate produced during daylight hours, because it is primarily formed through the reaction between NO_2 and photochemically produced ·OH:

$$NO + ·OH + M \rightarrow HNO_3 + M \qquad (R4)$$

We will refer to HNO_3 produced through R4 as $HNO_3(1)$ in the following discussion. Assuming no kinetic isotope fractionation associated with R4 (this will be discussed in a forth coming paper), the δ^x of $HNO_3(1)$ can be calculated using mass-balance as the following:

$$\delta^{15}N - HNO_3(1)(\text{‰}) = \delta^{15}N - NO_2(\text{‰}) \qquad (12)$$

$$\delta^{18}O - HNO_3(1)(\text{‰}) = \frac{2}{3}(\delta^{18}O - NO_2(\text{‰}))$$
$$+ \frac{1}{3}(\delta^{18}O - ·OH(\text{‰})) \qquad (13)$$

This model indicates that the N and O isotopic composition of $HNO_3(1)$ can be approximately calculated if δ^x-NO_2 and $\delta^{18}O$–·OH are known. Using this proposed model, we calculated daytime $\delta^{15}N$–NO_2 according to Eq. (10) assuming local $\delta^{15}N$–NO_x to range from -15–0‰ (Walters et al., 2015) and using N isotopic exchange fractionation factors for NO_2/NO from our previous study (Walters and Michalski, 2015). These NO_2/NO exchange fractionation factors were adapted to include corrections for ZPE anharmonicity (adapted $^{15}\beta$ and $^{15}\alpha_{NO2/NO}$ values can be found in Tables S5 and S6). Predicted daytime $\delta^{18}O$–NO_2 values, relative to VSMOW, were calculated from Eq. (10) assuming $\delta^{18}O$–NO_x to range from 112–122‰ (Michalski et al., 2014) and using O isotopic NO_2/NO exchange fractionation factors calculated in this
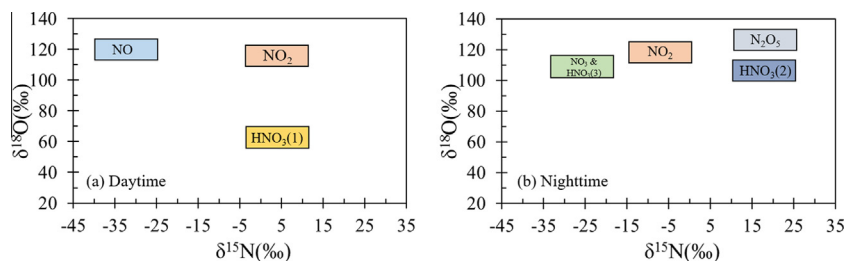
Fig. 4. Estimated $\delta^{18}O$–$\delta^{15}N$ compositions of several NO_y molecules assuming (a) daytime isotopic equilibrium between NO/NO_2 with $f_{NO2} = 0.7$ and (b) nighttime isotopic equilibrium between NO_2, NO_3, and N_2O_5. Where $HNO_3(1)$, $HNO_3(2)$, and $HNO_3(3)$ represent various HNO_3 production pathways that include $NO_2 + \cdot OH \rightarrow HNO_3(1)$, $N_2O_5 + H_2O + surface \rightarrow 2HNO_3(2)$, and $NO_3 + R \rightarrow HNO_3(3) + R\cdot$.

study. The $\delta^{18}O$ of $\cdot OH$ should to a first order approximation reflect the $\delta^{18}O$ of local water vapor and the temperature dependent fractionation factor associated with equilibrium $\cdot OH/H_2O$ exchange, since the atmospheric concentration of $\cdot OH$ is orders of magnitude lower than H_2O (Michalski et al., 2012):

$$\delta^{18}O - \cdot OH(\text{‰}) = \delta^{18}O - H_2O(\text{‰})$$
$$+ 1000\left(^{18}\alpha_{\cdot OH/H_2O} - 1\right) \qquad (14)$$

Therefore, $\delta^{18}O$ of $\cdot OH$ can be approximated using an estimated tropospheric water vapor $\delta^{18}O$ range of -25–0‰ (typical for mid-latitudes Michalski et al., 2012) and O isotopic $\cdot OH/H_2O$ exchange fractionation factors calculated in this study.

The predicted $\delta^{18}O$–$\delta^{15}N$ ranges of NO, NO_2, and $HNO_3(1)$ at 300 K with $f_{NO2} = 0.70$ exhibit significant variation (Fig. 4a). The $\delta^{15}N$ of $HNO_3(1)$ and NO_2 are calculated to range from -4.2–10.8‰, while $\delta^{15}N$ of NO is calculated to range from -40.2–-25.2‰. The positive shift in $\delta^{15}N$ of $HNO_3(1)$ and NO_2 and the negative shift in $\delta^{15}N$ of NO relative to the assumed $\delta^{15}N$–NO_x value (-15–0‰) is a direct result of the N isotopic exchange between NO and NO_2 that favors the partitioning of ^{15}N into NO_2 ($^{15}\alpha_{NO2/NO} = 1.0370$ at 300 K). The $\delta^{18}O$ of NO, NO_2, and $HNO_3(1)$ are estimated to range from 115.3–125.3‰, 109.5–119.5‰, and 52.8–67.8‰ at 300 K (Fig. 4a). The positive shift in $\delta^{18}O$ of NO and negative shift in NO_2 relative to the assumed initial $\delta^{18}O$–NO_x (112–122‰) is a result of their O isotopic exchange that favors the formation of ^{18}O in NO ($^{18}\alpha_{NO2/NO} = 0.992$ at 300 K). The estimated $\delta^{18}O$–$HNO_3(1)$ shift of -56.7‰ relative to NO_2 is a result of the 1/3 O contribution from $\cdot OH$ that is predicted to have a $\delta^{18}O$ range of -60.5–-35‰ due to its equilibration with H_2O at 300 K $^{18}\alpha_{\cdot OH/H_2O} = 0.9645$ at 300 K).

The impact of varying f_{NO2} values on NO and NO_2 isotopic exchange and its influence on $\delta^{15}N$ and $\delta^{18}O$ of NO,

NO_2, and $HNO_3(1)$ are displayed in Table 4. Generally, it is observed that $\delta^{15}N$ is highly sensitive to f_{NO2}, but $\delta^{18}O$ is not. For example, from $f_{NO2} = 1$ to $f_{NO2} = 0.55$, the shift in $\delta^{15}N$ of NO_2 and $HNO_3(1)$ is 16.3‰, while the change in $\delta^{18}O$ of NO_2 and $HNO_3(2)$ is -3.8‰ and -2.5‰, respectively (Table 4). The degree of sensitivity of $\delta^{15}N$ and $\delta^{18}O$ in $HNO_3(1)$ to f_{NO2} is a result of the magnitude of the NO_2/NO equilibrium fractionation factors, in which N fractionation is fairly large ($^{15}\alpha_{NO2/NO} = 1.0370$ at 300 K), while O fractionation is relatively minor ($^{18}\alpha_{NO2/NO} = 0.992$ at 300 K). This isotope equilibrium mechanism predicts that $\delta^{15}N$–$HNO_3(1)$ will be sensitive to diurnal fluctuations in f_{NO2}, which is a phenomenon that has been previously observed (Vicars et al., 2013). Additionally, this mechanism indicates that since O fractionation between NO and NO_2 is relatively minor, $\delta^{18}O$–$HNO_3(1)$ is approximately equal to the O isotope mass-balance between NO_x–O_3 (in photochemical equilibrium) and $\cdot OH$.

In addition to f_{NO2} dependence, the isotopic composition of $HNO_3(1)$ will also have a temperature dependence that is related to the temperature dependent $\alpha_{NO2/NO}$ and $\alpha_{\cdot OH/H_2O}$ values. As temperature decreases, $^{15}\alpha_{NO2/NO}$ increases (Walters and Michalski, 2015; Walters et al., 2016), and this will result in $HNO_3(1)$ having a higher $\delta^{15}N$ value relative to the $\delta^{15}N$–NO_x for a fixed f_{NO2} value. Additionally, while $^{18}\alpha_{NO2/NO}$ is relatively insensitive to temperature (Fig. 2), $^{18}\alpha_{\cdot OH/H_2O}$ values change significantly with temperature (i.e. $^{18}\alpha_{\cdot OH/H_2O} = 0.9494$ and 0.9682 at 220 K and 330 K, respectively). Therefore, the $\delta^{18}O$–$HNO_3(1)$ formed at lower temperatures will have a lower $\delta^{18}O$ that is primarily the result of the temperature dependence of isotopic exchange between $\cdot OH$ and H_2O for a fixed $\delta^{18}O$–H_2O. Overall, while it is difficult to predict the exact range of $\delta^{18}O$–$\delta^{15}N$ compositions of $HNO_3(1)$ due to its numerous dependences, the proposed mechanism predicts that $\delta^{15}N$–$HNO_3(1)$ should reflect $\delta^{15}N$–NO_2, which should be slightly higher than $\delta^{15}N$–NO_x; however,

Table 4
Shift in $\delta^{15}N$ and $\delta^{18}O$ of NO, NO_2, and $HNO_3(1)$ relative to NO_x as a function of f_{NO2}.

f_{NO2}	$\delta^{15}N$–NO	$\delta^{18}O$–NO	$\delta^{15}N$–NO_2	$\delta^{18}O$–NO_2	$\delta^{15}N$-$HNO_3(1)$	$\delta^{18}O$–$HNO_3(1)$
1	–	–	0	0	0	−57.5
0.85	−30.5	7.0	5.4	−1.2	5.4	−58.3
0.70	−25.3	5.8	10.8	−2.5	10.8	−59.2
0.55	−19.9	4.7	16.3	−3.8	16.3	−60.1

$\delta^{18}O$–$HNO_3(1)$ should be lower than $\delta^{18}O$–NO_2 as a result of the O isotopic mass-balance between NO_2 and $\cdot OH$.

4.2. Predicted nighttime HNO_3 $\delta^{18}O$–$\delta^{15}N$ space

During the nighttime, higher N oxides form and new pathways of HNO_3 production become important due to the absence of photochemically produced $\cdot OH$. Under these conditions, NO_2 is oxidized by O_3 forming the NO_3 radical R5, which exists at thermal equilibrium with NO_2 and N_2O_5 (Russell et al., 1985; R6). Subsequent hydrolysis of N_2O_5 on a wetted surface forms HNO_3.

$$NO_2 + O_3 \rightarrow NO_3 + O_2 \tag{R5}$$

$$NO_2 + NO_3 \leftrightarrow N_2O_5 \tag{R6}$$

$$N_2O_5 + H_2O + surface \rightarrow 2HNO_3 \tag{R7}$$

This HNO_3 formation pathway is typically most prevalent during the winter when N_2O_5 is thermally stable (Calvert et al., 1985; Chang et al., 2011). Nighttime HNO_3 may also form through hydrogen abstraction from organic compounds (R) by NO_3:

$$NO_3 + R \rightarrow HNO_3 + R\cdot \tag{R8}$$

Since photochemical cycling of NO_x shuts down during the night, nearly all NO_x exists as NO_2. Thus, δ^x-$NO_x \approx \delta^x$-NO_2 as isotopic exchange between NO and NO_2 ceases (Freyer et al., 1993; Walters et al., 2016). However, isotopic equilibrium between NO_2, NO_3, and N_2O_5 is likely to be achieved mirroring its rapid chemical equilibrium rate (lifetime of 1–2 min; Amell and Daniels, 1952; Freyer, 1991), which will have an impact on $\delta^{18}O$ and $\delta^{15}N$ of atmospheric nitrate produced during the night. Generally, the tropospheric concentrations of $[NO_2] \gg [N_2O_5] \geqslant [NO_3]$, as NO_2 is typically on the order of ppb while N_2O_5 and NO_3 are on the order of ppt (e.g. Chang et al., 2011). Therefore, in most cases the isotopic composition of N_2O_5 and NO_3 should reflect the exchange α's with respect to NO_2 (i.e. $\alpha_{N2O5/NO2}$ and $\alpha_{NO3/NO2}$) and can be determined from the following:

$$\delta^x - N_2O_5(‰) = \delta^x - NO_2(‰)$$
$$+ 1000 \left[{}^x\alpha_{N_2O_5/NO_2} - 1 \right] \tag{15}$$

$$\delta^x - NO_3(‰) = \delta^x - NO_2(‰)$$
$$+ 1000 \left[{}^x\alpha_{NO_3/NO_2} - 1 \right] \tag{16}$$

Assuming a negligible kinetic isotopic fractionation associated with R7, the isotopic composition of atmospheric nitrate produced through N_2O_5 hydrolysis, which we will refer to as $HNO_3(2)$, can be estimated from δ^x-N_2O_5 and O isotopic mass-balance, our calculated exchange fractionation factors, and using an estimated $\delta^{18}O$–H_2O range from −25–0‰.

$$\delta^{15}N - HNO_3(2)(‰) = \delta^{15}N - N_2O_5(‰) \tag{17}$$

$$\delta^{18}O - HNO_3(2)(‰) = \frac{5}{6} \left(\delta^{18}O - N_2O_5(‰) \right)$$
$$+ \frac{1}{6} \left(\delta^{18}O - H_2O(‰) \right) \tag{18}$$

Assuming this model, N_2O_5 and $HNO_3(2)$ have an estimated $\delta^{15}N$ range of 10.5–25.5‰ (Fig. 4b), which is approximately 25.5‰ higher than NO_x as a result of the

N_2O_5/NO_2 exchange ($^{15}\alpha_{N2O5/NO2} = 1.0255$ at 300 K). $\delta^{18}O$–N_2O_5 is estimated to range from 121.4–131.4‰ (Fig. 4b), as a result of the O isotopic exchange between N_2O_5/NO_2 ($^{18}\alpha_{N2O5/NO2} = 1.0094$ at 300 K). Assuming O mass-balance between N_2O_5 and H_2O (Eq. (18)), $\delta^{18}O$–$HNO_3(2)$ is predicted to range from 97.0–109.5‰ at 300 K. As temperatures decrease, the N and O fractionation from the N_2O_5/NO_2 isotopic exchange will increase, and this should result in higher δ^x-N_2O_5 relative to the local NO_x.

Nitrate produced at night formed through the NO_3 hydrogen abstraction pathway, which we will refer to as $HNO_3(3)$, will have an O and N isotopic composition that is equal to the isotopic composition of NO_3, assuming isotopic mass-balance and neglecting any kinetic isotopic fractionation associated with R8:

$$\delta^{15}N - HNO_3(3)(‰) = \delta^{15}N - NO_3(‰) \tag{19}$$

$$\delta^{18}O - HNO_3(3)(‰) = \delta^{18}O - NO_3(‰) \tag{20}$$

Assuming this isotopic mechanism, $\delta^{15}N$ of NO_3 and $HNO_3(3)$ are estimated to range from −33.1–−18.1‰, which is approximately 18.4‰ lower than the $\delta^{15}N$–NO_2 (Fig. 4b). Additionally, $\delta^{18}O$ of NO_3 and $HNO_3(3)$ is estimated to range from 102.9–112.9‰, which is approximately 9.7‰ lower than $\delta^{18}O$–NO_2 (Fig. 4b). Both $\delta^{15}N$ and $\delta^{18}O$ are lower in $HNO_3(3)$ relative to NO_2 due to isotopic exchange between NO_3 and NO_2 that favors both ^{15}N and ^{18}O partitioning in NO_2 ($^{15}\alpha_{NO3/NO2} = 0.9819$ and $^{18}\alpha_{NO3/NO2} = 0.9901$ at 300 K). Our calculations indicate that as temperatures decrease, both the N and O fractionation resulting from the NO_3/NO_2 isotopic exchange will increase, which will result in higher δ^x-$HNO_3(3)$ values.

It is important to note the uncertainty in the calculated $^x\beta$ of NO_3 that is related to the computational difficulties of NO_3 as previously discussed (e.g. Morris et al., 1990; Dutta et al., 2013). B3LYP/cc-pVTZ, EDF2/cc-pVTZ, and QCISD/cc-pVDZ models yielded $^{18}\beta$ within 3.8‰ at 300 K (Fig. 2) indicating general agreement. However, these methods found a wider range in $^{15}\beta$, from 1.0715 to 1.0864 at 300 K (Fig. S1), indicating a disagreement as high as 14.9‰. Despite the uncertainty in $^{15}\beta$ of NO_3, all of the considered computational methods indicate that the $^{15}\beta$ values of NO_3 are less than those of NO_2 (i.e. $^{15}\alpha_{NO3/NO2} < 1$; Fig. S2). Therefore, while the actual $^{15}\beta$ values of NO_3 are somewhat uncertain, our calculations indicate that NO_3 should have lower $\delta^{15}N$ relative to NO_2. In our calculations, we have used NO_3 $^{15}\beta$ and $^{18}\beta$ values calculated using EDF2/cc-pVTZ, because vibrational frequencies calculated with this method are in closer agreement with experimental data (Kim et al., 1992; Jacox and Thompson, 2008; Beckers et al., 2009) (Table 1).

4.3. Implications of $\delta^{18}O$–$\delta^{15}N$ compositions in HNO_3

Assuming the same range of starting N and O isotopic compositions of NO_x ($\delta^{15}N$–NO_x: −15–0‰, $\delta^{18}O$–NO_x: 112–122‰), our calculations suggest that different HNO_3 formation pathways yield relatively distinctive $\delta^{18}O$–$\delta^{15}N$ compositions (Fig. 5). Our calculations indicate that
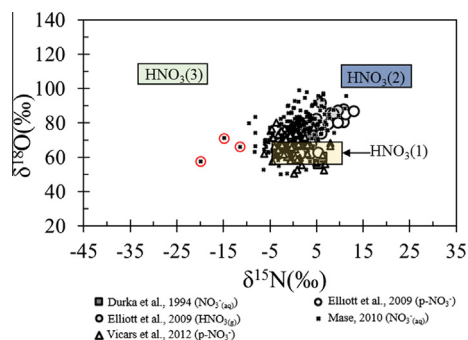
Fig. 5. Predicted $\delta^{18}O$–$\delta^{15}N$ compositions for three major HNO_3 production pathways that is compared with previous atmospheric nitrate measurements (Durka et al., 1994; Elliott et al., 2009; Mase, 2010; Vicars et al., 2013). Where $HNO_3(1)$, $HNO_3(2)$, and $HNO_3(3)$ represent various HNO_3 production pathways that include $NO_2 + \cdot OH \rightarrow HNO_3(1)$, $N_2O_5 + H_2O + \text{surface} \rightarrow 2HNO_3(2)$, and $NO_3 + R \rightarrow HNO_3(3) + R\cdot$. The data points within the red circles are outside of the predicted equilibrium $\delta^{18}O$–$\delta^{15}N$ space, which may indicate a NO_x source with an extremely low $\delta^{15}N$ value such as soil denitrification. (For interpretation of the references to colour in this figure legend, the reader is referred to the web version of this article.)

$HNO_3(1)$ should result in the lowest $\delta^{18}O$ values and mid-ranged $\delta^{15}N$ values. Our model predicts that $HNO_3(2)$ and $HNO_3(3)$ should have high $\delta^{18}O$ values that are similar. However, $HNO_3(2)$ has the highest predicted $\delta^{15}N$ values, while $HNO_3(3)$ has the lowest $\delta^{15}N$ values. This suggests that $\delta^{18}O$–$\delta^{15}N$ arrays for different HNO_3 production pathways can be used as isotopic end-members in isotope mixing models that might explain $\delta^{15}N$ and $\delta^{18}O$ values observed in atmospheric nitrate.

These predicted $\delta^{15}N$ and $\delta^{18}O$ isotopic end-members were compared with measured $\delta^{18}O$–$\delta^{15}N$ values of atmospheric nitrates (Fig. 5), including $HNO_{3(g)}$ (Elliott et al., 2009), p-NO_3^- (Elliott et al., 2009; Mase, 2010; Vicars et al., 2013), and $NO_{3(aq)}^-$ (Durka et al., 1994). The measured $\delta^{18}O$–$\delta^{15}N$ values in atmospheric nitrate plot between the two major HNO_3 formation pathways $HNO_3(1)$ and $HNO_3(2)$ predicted by this equilibrium model (Fig. 5). However, some of the reported $\delta^{18}O$–$\delta^{15}N$ values appear to represent a mixture of $HNO_3(1)$ and $HNO_3(3)$, which is most likely to occur for areas with high DMS/VOC concentrations such as marine and forest ecosystems (Geyer and Platt, 2002). Our predicted $\delta^{18}O$–$\delta^{15}N$ compositions may explain both the $\delta^{18}O$ and $\delta^{15}N$ seasonal cycling typically observed in atmospheric nitrate, in which $\delta^{18}O$ and $\delta^{15}N$ values are highest in the winter and lowest during the summer (e.g. Freyer, 1978, 1991; Elliott et al., 2009; Mase, 2010; Beyn et al., 2014). During winter, the $HNO_3(2)$ pathway is generally most prominent (Calvert et al., 1985; Chang et al., 2011), and our calculations suggest that this pathway results in high $\delta^{18}O$ and $\delta^{15}N$ values. During summer, the $HNO_3(1)$ pathway is generally most prominent due to the higher concentrations of photochemically produced $\cdot OH$ (Calvert et al., 1985), and our calculations suggest this pathway will result in $\delta^{15}N$

and $\delta^{18}O$ values lower than those for the $HNO_3(2)$ pathway.

While $\delta^{18}O$ and $\Delta^{17}O$ of atmospheric nitrate has been previously linked to NO_x oxidation pathways (e.g. Michalski et al., 2003, 2012; Savarino et al., 2007), our calculations suggest that $\delta^{15}N$ may also be linked to oxidation chemistry. However, seasonal changes in $\delta^{15}N$ of atmospheric nitrate will also be impacted by changes in seasonal emissions of NO_x by a variety of processes, particularly NO emitted by nitrification and denitrification occurring in soils. In areas where NO_x emissions should not change seasonally, such as areas dominated by fossil-fuel combustion, any observed seasonal change in $\delta^{15}N$ of atmospheric nitrate suggests seasonal changes in NO_x oxidation chemistry. In areas in which NO_x emissions exhibit a large seasonal change, such as agricultural regions, the $\delta^{15}N$ of atmospheric nitrate will be a function of both the seasonal change in $\delta^{15}N$–NO_x and in the NO_x oxidation equilibrium isotope effect. The equilibrium model indicates that it may be difficult to partition NO_x sources solely from $\delta^{15}N$–HNO_3 values, since the $\delta^{15}N$ tends to be sensitive to equilibrium effects that may alter the original NO_x source $\delta^{15}N$ value as it is oxidized to HNO_3 (Fig. 4). However, evaluation of $\delta^{15}N$–$\delta^{18}O$ space of atmospheric nitrate may help elucidate NO_x emission sources in some cases. Atmospheric nitrate outside of the calculated $\delta^{18}O$–$\delta^{15}N$ compositional range might indicate its NO_x precursor had a distinctive $\delta^{15}N$ outside of the typical range of -15 to $0‰$. For example, soil denitrification events, which are estimated to have a low $\delta^{15}N$–NO_x (approximately between -50 and $-20‰$; Li and Wang, 2008; Felix and Elliott, 2013, 2014) may be trackable with atmospheric nitrate $\delta^{18}O$–$\delta^{15}N$ measurements. If emitted NO_x is oxidized through the $HNO_3(1)$ pathway, it should have low $\delta^{15}N$ and $\delta^{18}O$, which does not match the equilibrium predictions (Fig. 5). This sort of event may explain why a few of the atmospheric nitrate measurements from Mase (2010) is outside of the general predicted HNO_3 formation $\delta^{18}O$–$\delta^{15}N$ range (Fig. 5). These rainwater nitrates were collected at N deposition sites after a storm saturated recently fertilized agricultural fields in the Midwestern U.S., suggesting NO produced by nitrification/denitrification.

While our predicted equilibrium $\delta^{18}O$–$\delta^{15}N$ compositions generally agrees with atmospheric nitrate measurements (e.g. Durka et al., 1994; Elliott et al., 2009; Mase, 2010; Vicars et al., 2013), it is important to point out the simplicity of our model. Primarily, we have ignored any kinetic isotope effects. If equilibrium between NO_2, NO_3, and N_2O_5 is achieved, kinetic isotope effects associated with the formation of NO_3 and N_2O_5 should be erased. However, kinetic isotopic effects will need to be considered for the photochemical cycling of NO_x, that includes NO_2 photolysis and NO oxidation, as these MDFPs are predicted to have an impact on the N and O isotopic composition of NO_2 (Walters et al., 2016), which may then be propagated into NO_y molecules. Additionally, we will need to determine kinetic isotope fractionation factors for the final step in forming atmospheric nitrate (i.e. R4, R7, and R8), which may play an important role in its N and O isotopic compo-

sition. Our equilibrium model suggests that the isotopic composition of NO_2 drives the isotopic composition of atmospheric nitrate indicating the need for future *in situ* isotopic measurements of NO_2. Determination of NO_x photochemical cycling fractionation factors, isotopic *in situ* measurements of NO_2, and kinetic isotopic modeling of NO_x oxidation will be the subject for future research.

5. CONCLUSIONS

Hybrid density functional theory calculations indicate that oxygen equilibrium isotopic exchange involving NO_y molecules generally favors the formation ^{18}O in NO_y molecules other than NO and NO_2 at the most likely O exchange sites. Therefore, equilibrium isotope exchange may play a role in the $\delta^{18}O$ of atmospheric nitrate in addition to the O isotopic mass-balance of its precursor molecules and oxidants. A simple equilibrium and mass-balance model indicates that the three major HNO_3 formation pathways may have unique $\delta^{18}O$–$\delta^{15}N$ compositions. This model generally predicts a range of $\delta^{18}O$–$\delta^{15}N$ values consistent with HNO_3 measurements and suggests that $\delta^{18}O$–$\delta^{15}N$ space of atmospheric nitrate may provide useful information about the conditions of NO_x oxidation pathways. This model may explain the seasonal changes typically observed in both $\delta^{18}O$ and $\delta^{15}N$ of atmospheric nitrate.

APPENDIX A. SUPPLEMENTARY DATA

Supplementary data associated with this article can be found, in the online version, at http://dx.doi.org/10.1016/j.gca.2016.06.039.

REFERENCES

Alexander B. and Mickley L. J. (2015) Paleo-perspectives on potential future changes in the oxidative capacity of the atmosphere due to climate change and anthropogenic emissions. *Curr. Pollut. Rep.*, 1–13.

Alexander B., Hastings M. G., Allman D. J., Dachs J., Thornton J. A. and Kunasek S. A. (2009) Quantifying atmospheric nitrate formation pathways based on a global model of the oxygen isotopic composition ($\Delta^{17}O$) of atmospheric nitrate. *Atmos. Chem. Phys.* **9**, 5043–5056.

Amell A. R. and Daniels F. (1952) Kinetics of the exchange of N^{15} between $N^{15}O_2$ and N_2O_5. *J. Am. Chem. Soc.* **74**, 6209–6212.

Anbar A. D., Jarzecki A. A. and Spiro T. G. (2005) Theoretical investigation of iron isotope fractionation between $Fe(H_2O)_6^{3+}$ and $Fe(H_2O)_6^{2+}$: Implications for iron stable isotope geochemistry. *Geochim. Cosmochim. Acta* **69**, 825–837.

Becke A. D. (1993) Density-functional thermochemistry. III. The role of exact exchange. *J. Chem. Phys.* **98**, 5648–5652.

Beckers H., Willner H. and Jacox M. E. (2009) Conflicting observations resolved by a far IR and UV/Vis study of the NO_3 radical. *ChemPhysChem* **10**, 706–710.

Berhanu T. A., Savarino J., Bhattacharya S. K. and Vicars W. C. (2012) ^{17}O excess transfer during the $NO_2 + O_3 \rightarrow NO_3 + O_2$ reaction. *J. Chem. Phys.* **136**, 044311.

Beyn F., Matthias V. and Dähnke K. (2014) Changes in atmospheric nitrate deposition in Germany – an isotopic perspective. *Environ. Pollut.* **194**, 1–10.

Bigeleisen J. and Mayer M. G. (1947) Calculation of equilibrium constants for isotopic exchange reactions. *J. Chem. Phys.* **15**, 261–267.

Böhlke J. K., Mroczkowski S. J. and Coplen T. B. (2003) Oxygen isotopes in nitrate: new reference materials for ^{18}O: ^{17}O: ^{16}O measurements and observations on nitrate-water equilibration. *Rapid Commun. Mass Spectrom.* **17**, 1835–1846.

Calvert J. G., Lazrus A., Kok G. L., Heikes B. G., Walega J. G., Lind J. and Cantrell C. A. (1985) Chemical mechanisms of acid generation in the troposphere. *Nature* **317**, 27–35.

Chang W. L., Bhave P. V., Brown S. S., Riemer N., Stutz J. and Dabdub D. (2011) Heterogeneous atmospheric chemistry, ambient measurements, and model calculations of N_2O_5: a review. *Aerosol Sci. Technol.* **45**, 665–695.

Coulson D. R. (1978) Statistical factors in reaction rate theories. *J. Am. Chem. Soc.* **100**, 2992–2996.

Driesner T., Ha T. K. and Seward T. M. (2000) Oxygen and hydrogen isotope fractionation by hydration complexes of Li^+, Na^+, K^+, Mg^{2+}, F^-, Cl^-, and Br^-: a theoretical study. *Geochim. Cosmochim. Acta* **64**, 3007–3033.

Dubey M. K., Mohrschladt R., Donahue N. M. and Anderson J. G. (1997) Isotope specific kinetics of hydroxyl radical (OH) with water (H_2O): testing models of reactivity and atmospheric fractionation. *J. Phys. Chem. A* **101**, 1494–1500.

Dunning T. H. (1989) Gaussian basis sets for use in correlated molecular calculations. I. The atoms boron through neon and hydrogen. *J. Chem. Phys.* **90**, 1007–1023.

Durka W., Schulze E.-D., Gebauer G. and Voerkeliust S. (1994) Effects of forest decline on uptake and leaching of deposited nitrate determined from ^{15}N and ^{18}O measurements. *Nature* **372**, 765–767.

Dutta A. K., Vaval N. and Pal S. (2013) Performance of the EOMIP-CCSD(2) method for determining the structure and properties of doublet radicals: a benchmark investigation. *J. Chem. Theory Comput.* **9**, 4313–4331.

Elliott E. M., Kendall C., Boyer E. W., Burns D. A., Lear G. G., Golden H. E., Harlin K., Bytnerowicz A., Butler T. J. and Glatz R. (2009) Dual nitrate isotopes in dry deposition: utility for partitioning NO_x source contributions to landscape nitrogen deposition. *J. Geophys. Res. Biogeosciences* **114**, G04020.

Felix J. D. and Elliott E. M. (2013) The agricultural history of human-nitrogen interactions as recorded in ice core $\delta^{15}N$–NO_3^-. *Geophys. Res. Lett.* **40**, 1642–1646.

Felix J. D. and Elliott E. M. (2014) Isotopic composition of passively collected nitrogen dioxide emissions: vehicle, soil and livestock source signatures. *Atmos. Environ.* **92**, 359–366.

Freyer H. D. (1978) Seasonal trends of NH_4^+ and NO_3^- nitrogen isotope composition in rain collected at Jülich, Germany. *Tellus* **30**, 83–92.

Freyer H. D. (1991) Seasonal variation of $^{15}N/^{14}N$ ratios in atmospheric nitrate species. *Tellus B* **43**, 30–44.

Freyer H. D., Kley D., Volz-Thomas A. and Kobel K. (1993) On the interaction of isotopic exchange processes with photochemical reactions in atmospheric oxides of nitrogen. *J. Geophys. Res.* **98**, 14791–14796.

Frisch M. J., Trucks G. W., Schlegel H. B., Scuseria G. E., Robb M. A., Cheeseman J. R., Scalmani G., Barone V., Mennucci B., Petersson G. A., Nakatsuji H., Caricato M., Li X., Hratchian H. P., Izmaylov A. F., Bloino J., Zheng G., Sonnenberg J. L., Hada M., Ehara M., Toyota K., Fukuda R., Hasegawa J., Ishida M., Nakajima T., Honda Y., Kitao O., Nakai H., Vreven T., Montgomery, Jr, J. A., Peralta J. E., Ogliaro F., Bearpark M., Heyd J. J., Brothers E., Kudin K. N., Staroverov V. N., Kobayashi R., Normand J., Raghavachari K., Rendell A., Burant J. C., Iyengar S. S., Tomasi J., Cossi M., Rega N., Milliam J. M., Klene M., Knox J. E., Cross J. B., Bakken V., Adamo C., Jaramillo J., Gomperts R., Stratmann R. E., Yazyev O., Austin A. J., Cammi R., Pomelli C., Ochterski J. W., Martin R. L., Morokuma K., Zakrzewski V. G., Voth G. A., Salvador P., Dannenberg J. J., Dapprich S., Daniels A. D., Farkas Ö., Foresman J. B., Ortiz J. V., Cioslowski J. and Fox D. J. (2009) *Gaussian 09, Revision D.01*. Gaussian Inc, Wallingford, CT.

Gao H. O. (2007) Day of week effects on diurnal ozone/NO$_x$ cycles and transportation emissions in Southern California. *Transp. Res. Part Transp. Environ.* **12**, 292–305.

Geyer A. and Platt U. (2002) Temperature dependence of the NO$_3$ loss frequency: a new indicator for the contribution of NO$_3$ to the oxidation of monoterpenes and NO$_x$ removal in the atmosphere. *J. Geophys. Res. Atmospheres* **107**, D20.

Jacox M. E. and Thompson W. E. (2008) The infrared spectroscopy and photochemistry of NO$_3$ trapped in solid neon. *J. Chem. Phys.* **129**, 204306.

Johnston J. C. and Thiemens M. H. (1997) The isotopic composition of tropospheric ozone in three environments. *J. Geophys. Res. Atmospheres* **1984–2012**(102), 25395–25404.

Kim B., Hunter P. L. and Johnston H. S. (1992) NO3 radical studied by laser-induced fluorescence. *J. Chem. Phys.* **96**, 4057–4067.

Krankowsky D., Bartecki F., Klees G. G., Mauersberger K., Schellenbach K. and Stehr J. (1995) Measurement of heavy isotope enrichment in tropospheric ozone. *Geophys. Res. Lett.* **22**, 1713–1716.

Lee C., Yang W. and Parr R. G. (1988) Development of the Colle-Salvetti correlation-energy formula into a functional of the electron density. *Phys. Rev. B* **37**, 785.

Leighton P. (1961) *Photochemistry of Air Pollution*. Academic, New York.

Li D. and Wang X. (2008) Nitrogen isotopic signature of soil-released nitric oxide (NO) after fertilizer application. *Atmos. Environ.* **42**, 4747–4754.

Lin C. Y., George M. W. and Gill P. M. (2004) EDF2: A density functional for predicting molecular vibrational frequencies. *Aust. J. Chem.* **57**, 365–370.

Liu Y. and Tossell J. A. (2005) Ab initio molecular orbital calculations for boron isotope fractionations on boric acids and borates. *Geochim. Cosmochim. Acta* **69**, 3995–4006.

Liu Q., Tossell J. A. and Liu Y. (2010) On the proper use of the Bigeleisen–Mayer equation and corrections to it in the calculation of isotopic fractionation equilibrium constants. *Geochim. Cosmochim. Acta* **74**, 6965–6983.

Lyons J. R. (2001) Transfer of mass-independent fractionation in ozone to other oxygen-containing radicals in the atmosphere. *Geophys. Res. Lett.* **28**, 3231–3234.

Mase D. F. (2010) *A Coupled Modeling and Observational Approach to Understanding Oxygen-18 in Atmospheric Nitrate*. Purdue University.

Mauersberger K., Lämmerzahl P. and Krankowsky D. (2001) Stratospheric ozone isotope enrichments—revisited. *Geophys. Res. Lett.* **28**, 3155–3158.

McCabe J. R., Thiemens M. H. and Savarino J. (2007) A record of ozone variability in South Pole Antarctic snow: Role of nitrate oxygen isotopes. *J. Geophys. Res. Atmospheres* **112**, D12303.

Michalski G. (2003) *Isotopic studies of nitrate and nitrogen dioxide: atmospheric and biosphere N cycling*. University of California, San Diego.

Michalski G. and Bhattacharya S. K. (2009) The role of symmetry in the mass independent isotope effect in ozone. *Proc. Natl. Acad. Sci.* **106**, 5493–5496.

Michalski G., Bhattacharya S. K. and Mase D. F. (2012) Oxygen isotope dynamics of atmospheric nitrate and its precursor molecules. In *Handbook of Environmental Isotope Geochemistry*. Springer, pp. 613–635.

Michalski G., Bhattacharya S. K. and Girsch G. (2014) NO$_x$ cycle and the tropospheric ozone isotope anomaly: an experimental investigation. *Atmos. Chem. Phys.* **14**, 4935–4953.

Michalski G., Jost R., Sugny D., Joyeux M. and Thiemens M. (2004) Dissociation energies of six NO$_2$ isotopologues by laser induced fluorescence spectroscopy and zero point energy of some triatomic molecules. *J. Chem. Phys.* **121**, 7153–7161.

Michalski G., Scott Z., Kabiling M. and Thiemens M. H. (2003) First measurements and modeling of Δ^{17}O in atmospheric nitrate. *Geophys. Res. Lett.* **30**, 1870.

Monse E. U., Spindel W. and Stern M. J. (1969) Analysis of isotope-effect calculations illustrated with exchange equilibria among oxynitrogen compounds. *ACS Adv. Chem.* **89**, 148–184.

Morin S., Savarino J., Frey M. M., Yan N., Bekki S., Bottenheim J. W. and Martins J. M. (2008) Tracing the origin and fate of NO$_x$ in the Arctic atmosphere using stable isotopes in nitrate. *Science* **322**, 730–732.

Morris V. R., Bhatia S. C. and Hall J. H. (1990) *Ab initio* self-consistent field study of the vibrational spectra for nitrate radical geometric isomers. *J. Phys. Chem.* **94**, 7414–7418.

Otake T., Lasaga A. C. and Ohmoto H. (2008) Ab initio calculations for equilibrium fractionations in multiple sulfur isotope systems. *Chem. Geol.* **249**, 357–376.

Pennington R. E. and Kobe K. A. (1954) Contributions of vibrational anharmonicity and rotation–vibration interaction to thermodynamic functions. *J. Chem. Phys.* **22**, 1442–1447.

Pollak E. L. I. and Pechukas P. (1978) Symmetry numbers, not statistical factors, should be used in absolute rate theory and in Broensted relations. *J. Am. Chem. Soc.* **100**, 2984–2991.

Purdue Radon Cluster ITaP Research Computing – Radon. Available at: https://www.rcac.purdue.edu/compute/radon/ (accessed 4.05.15).

Redlich O. (1935) Eine allgemeine Beziehung zwischen den Schwingungsfrequenzen isotoper Molekeln. *Z. Phys. Chem B* **28**, 371–382.

Richet P., Bottinga Y. and Janoy M. (1977) A review of hydrogen, carbon, nitrogen, oxygen, sulphur, and chlorine stable isotope enrichment among gaseous molecules. *Annu. Rev. Earth Planet. Sci.* **5**, 65–110.

Riha K. M. (2013) *The Use of Stable Isotopes to Constrain The Nitrogen Cycle*. Purdue University.

Russell A. G., McRae G. J. and Cass G. R. (1985) The dynamics of nitric acid production and the fate of nitrogen oxides. *Atmos. Environ. (1967)* **19**, 893–903.

Savarino J., Kaiser J., Morin S., Sigman D. M. and Thiemens M. H. (2007) Nitrogen and oxygen isotopic constraints on the origin of atmospheric nitrate in coastal Antarctica. *Atmos. Chem. Phys.* **7**, 1925–1945.

Savarino J., Bhattacharya S. K., Morin S., Baroni M. and Doussin J.-F. (2008) The NO + O$_3$ reaction: a triple oxygen isotope perspective on the reaction dynamics and atmospheric implications for the transfer of the ozone isotope anomaly. *J. Chem. Phys.* **128**, 194303.

Savarino J., Morin S., Erbland J., Grannec F., Patey M. D., Vicars W., Alexander B. and Achterberg E. P. (2013) Isotopic composition of atmospheric nitrate in a tropical marine boundary layer. *Proc. Natl. Acad. Sci.* **110**, 17668–17673.

Schauble E. A., Ghosh P. and Eiler J. M. (2006) Preferential formation of ^{13}C–^{18}O bonds in carbonate minerals, estimated using first-principles lattice dynamics. *Geochim. Cosmochim. Acta* **70**, 2510–2529.

Schauble E., Rossman G. R. and Taylor H. P. (2004) Theoretical estimates of equilibrium chromium-isotope fractionations. *Chem. Geol.* **205**, 99–114.

Scott A. P. and Radom L. (1996) Harmonic vibrational frequencies: an evaluation of Hartree-Fock, Møller-Plesset, quadratic configuration interaction, density functional theory, and semiempirical scale factors. *J. Phys. Chem.* **100**, 16502–16513.

Shao Y., Gan Z., Epifanovsky E., Gilbert A. T. B., Wormit M., Kussmann J., Lange A. W., Behn A., Deng J., Feng X., Ghosh D., Goldey M., Horn P. R., Jacobson L. D., Kaliman I., Khaliullin R. Z., Kuś T., Landau A., Liu J., Proynov E. I., Rhee Y. M., Richard R. M., Rohrdanz M. A., Steele R. P., Sundstrom E. J., Woodcock H. L., Zimmerman P. M., Zuev D., Albrecht B., Alguire E., Austin B., Beran G. J. O., Bernard Y. A., Berquist E., Brandhorst K., Bravaya K. B., Brown S. T., Casanova D., Chang C.-M., Chen Y., Chien S. H., Closser K. D., Crittenden D. L., Diedenhofen M., DiStasio R. A., Do H., Dutoi A. D., Edgar R. G., Fatehi S., Fusti-Molnar L., Ghysels A., Golubeva-Zadorozhnaya A., Gomes J., Hanson-Heine M. W. D., Harbach P. H. P., Hauser A. W., Hohenstein E. G., Holden Z. C., Jagau T.-C., Ji H., Kaduk B., Khistyaev K., Kim J., Kim J., King R. A., Klunzinger P., Kosenkov D., Kowalczyk T., Krauter C. M., Lao K. U., Laurent A. D., Lawler K. V., Levchenko S. V., Lin C. Y., Liu F., Livshits E., Lochan R. C., Luenser A., Manohar P., Manzer S. F., Mao S.-P., Mardirossian N., Marenich A. V., Maurer S. A., Mayhall N. J., Neuscamman E., Oana C. M., Olivares-Amaya R., O'Neill D. P., Parkhill J. A., Perrine T. M., Peverati R., Prociuk A., Rehn D. R., Rosta E., Russ N. J., Sharada S. M., Sharma S., Small D. W., Sodt A., Stein T., Stück D., Su Y.-C., Thom A. J. W., Tsuchimochi T., Vanovschi V., Vogt L., Vydrov O., Wang T., Watson M. A., Wenzel J., White A., Williams C. F., Yang J., Yeganeh S., Yost S. R., You Z.-Q., Zhang I. Y., Zhang X., Zhao Y., Brooks B. R., Chan G. K. L., Chipman D. M., Cramer C. J., Goddard W. A., Gordon M. S., Hehre W. J., Klamt A., Schaefer H. F., Schmidt M. W., Sherrill C. D., Truhlar D. G., Warshel A., Xu X., Aspuru-Guzik A., Baer R., Bell A. T., Besley N. A., Chai J.-D., Dreuw A., Dunietz B. D., Furlani T. R., Gwaltney S. R., Hsu C.-P., Jung Y., Kong J., Lambrecht D. S., Liang W., Ochsenfeld C., Rassolov V. A., Slipchenko L. V., Subotnik J. E., Van Voorhis T., Herbert J. M., Krylov A. I., Gill P. M. W. and Head-Gordon M. (2015) Advances in molecular quantum chemistry contained in the Q-Chem 4 program package. *Mol. Phys.* **113**, 184–215.

Sharma H. D., Jervis R. E. and Wong K. Y. (1970) Isotopic exchange reactions in nitrogen oxides. *J. Phys. Chem.* **74**, 923–933.

Sinha P., Boesch S. E., Gu C., Wheeler R. A. and Wilson A. K. (2004) Harmonic vibrational frequencies: scaling factors for HF, B3LYP, and MP2 methods in combination with correlation consistent basis sets. *J. Phys. Chem. A* **108**, 9213–9217.

Stern M. J., Spindel W. and Monse E. U. (1968) Temperature dependences of isotope effects. *J. Chem. Phys.* **48**, 2908–2919.

Thiemens M. H. (2006) History and applications of mass-independent isotope effects. *Annu. Rev. Earth Planet Sci.* **34**, 217–262.

Thiemens M. H. and Heidenreich J. E. (1983) The mass-independent fractionation of oxygen: a novel isotope effect and its possible cosmochemical implications. *Science* **219**, 1073–1075.

Urey H. C. (1947) The thermodynamic properties of isotopic substances. *J. Chem. Soc.* **7**, 562–581.

Vicars W. C. and Savarino J. (2014) Quantitative constraints on the ^{17}O-excess ($\Delta^{17}O$) signature of surface ozone: Ambient measurements from 50° N to 50° S using the nitrite-coated filter technique. *Geochim. Cosmochim. Acta* **135**, 270–287.

Vicars W. C., Bhattacharya S. K., Erbland J. and Savarino J. (2012) Measurement of the ^{17}O-excess ($\Delta^{17}O$) of tropospheric ozone using a nitrite-coated filter. *Rapid Commun. Mass Spectrom.* **26**, 1219–1231.

Vicars W. C., Morin S., Savarino J., Wagner N. L., Erbland J., Vince E., Martins J. M. F., Lerner B. M., Quinn P. K. and Coffman D. J. (2013) Spatial and diurnal variability in reactive nitrogen oxide chemistry as reflected in the isotopic composition of atmospheric nitrate: Results from the CalNex 2010 field study. *J. Geophys. Res. Atmospheres* **118**, 10567–10588.

Walters W. W. and Michalski G. (2015) Theoretical calculation of nitrogen isotope equilibrium exchange fractionation factors for various NO_y molecules. *Geochim. Cosmochim. Acta* **164**, 284–297.

Walters W. W., Simonini D. S. and Michalski G. (2016) Nitrogen isotope exchange between NO and NO_2 and its implications for $\delta^{15}N$ variations in tropospheric NO_x and atmospheric nitrate. *Geophys. Res. Lett.* **43**, 440–448.

Walters W. W., Tharp B. D., Fang H., Kozak B. J. and Michalski G. (2015) Nitrogen isotope composition of thermally produced NO_x from various fossil-fuel combustion sources. *Environ. Sci. Technol.* **49**, 11353–11371.

Yamaji K., Makita Y., Watanabe H., Sonoda A., Kanoh H., Hirotsu T. and Ooi K. (2001) Theoretical estimation of lithium isotopic reduced partition function ratio for lithium ions in aqueous solution. *J. Phys. Chem. A* **105**, 602–613.

Associate editor: Edwin Schauble